OPTIMIZATION AND THE MIRANDA APPROACH IN DETECTING HORSESHOE-TYPE CHAOS BY COMPUTER

BALÁZS BÁNHELYI, TIBOR CSENDES*, and
BARNABAS M. GARAY†
Institute of Informatics, University of Szeged,
H-6701 Szeged P.O. Box 652, Hungary;
**csendes@inf.u-szeged.hu*
†*Department of Mathematics, Budapest University of Technology,*
H-1521 Budapest, Hungary

Received February 8, 2006; Revised ...

We report on experiences with an adaptive subdivision method supported by interval arithmetic that enables us to prove subset relations of the form $\mathcal{T}(W) \subset U$ and thus to check certain sufficient conditions for chaotic behaviour of dynamical systems in a rigorous way.

Our proof of the underlying abstract theorem avoids of referring to any results of applied algebraic topology and relies only on the Brouwer fixed point theorem.

The second novelty is that the process of gaining the subset relations to be checked is, to a large extent, also automatized. The promising subset relations come from solving a constrained optimization problem via the penalty function approach.

Abstract results and computational methods are demonstrated by finding embedded copies of the standard horseshoe dynamics in iterates of the classical Hénon mapping.

Keywords: Smale horseshoe, chaos, Hénon–mapping, computer–aided proof, verified global optimization.

1 Introduction

The establishing of computer-assisted proofs for chaos is one of the great success stories of dynamical systems theory in the last decade. The high-points of this development are the Mischaikow-Mrozek proof for the existence of a topological horseshoe [Mischaikow & Mrozek, 1995] and the Tucker proof for the existence of a strange attractor [Tucker, 1999] in the Lorenz system. Roughly speaking, a computer-assisted proof for chaos is a mixture of

- *a* THEORETICAL PART: the establishing of a sufficient condition for (a certain type of) chaos that consists of a finite collection of inclusions of the form $\mathcal{T}_j(W_j) \subset U_j$ where the W_j's and the U_j's are subsets of the phase space and the $\mathcal{T}_j$'s are functions associated with the dynamics,

- *and of a* COMPUTATIONAL PART: the verification of these inclusions by a rigorous numerical method that consists of finding the W_j's and the U_j's as well as of the verified checking of the relations $\mathcal{T}_j(W_j) \subset U_j$, $j = 1, 2, \ldots, M$.

The collection of of the subset relations $\mathcal{T}_j(W_j) \subset U_j$, $j = 1, 2, \ldots, M$ forms a sufficient condition for chaos in a region determined by the subset relations themselves. In order to locate chaotic regions, one has to find the subset relations to be checked. In [Mischaikow & Mrozek, 1995] and in [Tucker, 1999], the W_j's and the U_j's are subsets of suitable Poincarè sections of the dynamics and the $\mathcal{T}_j$'s are the corresponding return/Poincarè maps. Everywhere in the literature we are aware of, the successful triplets $\{(\mathcal{T}_j, W_j, U_j)\}_{j=1}^{M}$ are found as a result of computer experimentation with human overhead, i.e., in a final analysis, by hand.

Much less human interaction is needed when the possible subset relations are assumed to depend on certain parameters. Undoubtfully, the choice of the parameter space Λ requires an "intelligent guess", exploiting numerical and theoretical results on the dynamics. However, the task of finding a particular parameter value $\lambda_0 \in \Lambda$ for which the subset relations $\mathcal{T}_j(\lambda_0)(W_j(\lambda_0)) \subset U_j(\lambda_0)$, $j = 1, 2, \ldots, M$ are all satisfied — this tedious task is the terrain of optimization methods and can be left entirely to the computer.

As we shall see in the next subsec., the core of detecting horseshoe-type chaos is to find periodic points with prescribed left-right itinaries. Periodic points with prescribed left-right itinaries are fixed points for iterated functions on certain product spaces. This is how fixed point theory leads to horseshoe-type chaos, a dynamics at least as complicated as the one of the

shift operator on the space of two symbols. The proof of the underlying abstract [Zgliczynski, 1996] result, itself a simplification of the Conley index argument [Mischaikow-Mrozek, 1995], is simplified further by observing that fixed-point index and/or degree arguments can be replaced by applying the more elementary Brouwer fixed point theorem.

The paper is organized as follows. The next section is devoted to the subset relations to be checked. Subsec. 2.1 is also of introductory character. The simplified proof of Zgliczynski's theorem is given in Subsec. 2.2, his horseshoe found in the dynamics of the seventh iterate of the classical Hénon mapping is reconsidered in Subsec. 2.3. Our verified checking algorithm and the optimization model are presented in Section 3. Subsec. 3.3. contains a variety of rigorous numerical chaos results for iterates of the family of Hénon mappings.

2 Theoretical Results

2.1 The definition of horseshoe-type L–R chaos

Let X be a metric space, $L \neq \emptyset$ and $R \neq \emptyset$ be disjoint compact subsets of X, and let $\varphi : L \cup R \to X$ be a continuous mapping. For brevity, we say that $\{Q_{\gamma_k}\}_{k\in\mathbf{Z}}$ is a doubly infinite L–R sequence if $\{\gamma_k\}_{k\in\mathbf{Z}}$ is a doubly infinite 0–1 sequence (with $\gamma_k \in \{0,1\}$ for $k \in \mathbf{Z}$) and $Q_0 = L$, $Q_1 = R$. Finally, we say that φ *has a horseshoe-type* L–R *chaos in* X if, given a doubly infinite L–R sequence $\{Q_{\gamma_k}\}_{k\in\mathbf{Z}}$ arbitrarily, there exists a doubly infinite sequence of points $\{x_k\}_{k\in\mathbf{Z}} \subset X$ with the properties that $x_{k+1} = \varphi(x_k)$ and $x_k \in Q_{\gamma_k}$ for each $k \in \mathbf{Z}$. Letters L and R are chosen to indicate that, when drawing figures and thus visualizing the results below, the sets $Q_0 = L$ and $Q_1 = R$ are placed on the left half and the right half of those figures, respectively. Hence L–R chaos is an abbreviation for left–right chaos and refers to the set $L \cup R$ as to a chaotic region or, more precisely, as to a subset of the phase space containing a certain type of chaotic behaviour. For horseshoes and chaos in general (as well as for the concept of topological entropy we use in the last paragraph of Subsec. 3.3.2 below), see [Robinson, 1999] and [Wiggins, 2003].

Given a multiindex $\alpha = (\alpha_0, \alpha_1, \ldots, \alpha_N)$ with $\alpha_k \in \{0,1\}$ for $k = 0, 1, \ldots, N$ ($N \in \mathbf{N}$), set $Q_\alpha = Q_{\alpha_0} \times Q_{\alpha_1} \times \cdots \times Q_{\alpha_N}$ and consider the mapping

$$\Phi_\alpha : Q_\alpha \to Q_\alpha, \quad q = (q_0, q_1, \ldots, q_N) \to \Phi_\alpha(q),$$

$$(\Phi_\alpha(q))_k = \varphi(q_N) \text{ if } k = 0 \text{ and } \varphi(q_{k-1}) \text{ if } k = 1, \ldots, N. \qquad (1)$$

Theorem 1 *Suppose that*

$$\text{given an arbitrary multiindex } \alpha, \Phi_\alpha \text{ has a fixed point in } Q_\alpha. \tag{2}$$

Then φ has a horseshoe-type L–R chaos in X.

Proof. Consider a 0–1 index sequence $\{\gamma_k\}_{k\in\mathbf{Z}}$. Note that $q = \Phi_\alpha(q)$ if and only if $q_k = \varphi(q_0) \in Q_{\alpha_k}$ for $k = 0, 1, \ldots, N$ and $\varphi^{N+1}(q_0) = q_0$. Consequently, in view of condition (2), there exists a (2ℓ)-periodic sequence of points $\{x_k\}_{k\in\mathbf{Z}} \subset X$ with the properties

$$x^\ell_{-\ell+k} = \varphi^k(x^\ell_{-\ell}) \quad \text{for} \quad k = 0, 1, \ldots, 2\ell \quad \text{and} \quad \ell = 1, 2, \ldots \text{ and}$$

$$x^\ell_{-\ell+k} = Q_{\gamma_{-\ell+k}} \quad \text{for} \quad k = 0, 1, \ldots, 2\ell - 1 \quad \text{and} \quad \ell = 1, 2, \ldots.$$

Passing to consecutive subsequences, we can see that there is no loss of generality when we assume that $x^\ell_{-j} \to x^*_{-j}$ as $\ell \to \infty$, for each $j \in \mathbf{N}$. For $j = 1, 2, \ldots$, set $x^*_j = \varphi^j(x^*_0)$. By the construction, $x^*_{j+1} = \varphi(x^*_j) \in Q_{\gamma_{j+1}}$, $j \in \mathbf{Z}$. □

2.2 Practical criteria for horseshoe-type L–R chaos

It is fundamental that condition (2) — which is in fact an infinite collection of individual conditions — is a consequence of a finite number of inclusions appropriately chosen.

The derivation of condition (2) from the underlying finite collection of inclusions is furnished by topological fixed point arguments. This is fairly easy in one dimension and belongs to the elements of the theory of interval maps [Robinson, 1999]. The proof is given here only for convenience.

Theorem 2 *Let $X = \mathbf{R}$ and let L and R be disjoint compact intervals in X. Finally, let $\varphi : L \cup R \to X$ be a continuous mapping. Then condition (2) is the consequence of inclusions $L \cup R \subset \varphi(L)$ and $L \cup R \subset \varphi(R)$.*

Proof. In fact, let J_{α_N} be a closed subinterval of Q_{α_N} such that $\varphi(J_{\alpha_N}) = Q_{\alpha_0}$. The existence of J_{α_N} follows from an elementary connectedness argument in one dimension. Similarly, for $k = N-1, \ldots, 1, 0$ there exists a closed subinterval J_{α_k} of Q_{α_k} with the property that $\varphi(J_{\alpha_k}) = J_{\alpha_{k+1}}$. For $k = 0$, we conclude that $\varphi^{N+1}(J_{\alpha_0}) = Q_{\alpha_0} \supset J_{\alpha_0}$. By a simple fixed point argument in one dimension, $q_0 = \varphi^{N+1}(q_0)$ for some $q_0 \in J_{\alpha_0}$. By the construction, $q_k = \varphi^k(q_0) \in J_{\alpha_k} \subset Q_{\alpha_k}$ for $k = 0, 1, \ldots, N$. Thus

$q = (q_0, q_1, \ldots, q_N) \in Q_\alpha$ is a solution of equation $q = \Phi_\alpha(q)$. □

In higher dimension, however, condition (2) seems to have appeared only in connection with the first computer-assisted proofs for complicated dynamical behaviour. We restrict ourselves to present a model theorem in two dimension which is, up to a self–homeomorphism of $\mathbf{R}^2$, equivalent to a simplified version of the main result in [Zgliczynski, 1996] on what he calls φ–coverings with transition matrix $T = \{t_{i,j}\}_{i,j=0}^{1}$, $t_{i,j} = 1$, $i, j = 0, 1$, the transition matrix of the standard horseshoe dynamics (full shift on two symbols). The more recent development [Wójcik & Zgliczynski, 2000], [Galias & Zgliczynski, 2001], [Gidea & Zgliczynski, 2004] witnessed various combinatorial versions of condition (2) and refinements of the underlying finite collection of inclusions. The $\{Q_0, Q_1\}$ pair was replaced by the n-tuple $\{Q_0, Q_1, \ldots, Q_n\}$ of pairwise disjoint subsets, $\{0, 1\}^{N+1}$ as the set of multiindices in (2) was replaced by certain subsets of $\{0, 1, \ldots, n\}^{N+1}$ etc. but the geometry of the underlying inclusions preserved its rectangular character.

Theorem 3 *Set $X = \mathbf{R}^2$. With $x = (x_1, x_2) \in \mathbf{R} \times \mathbf{R} = X$, define*

$$E = \{x \in X \mid 1 \le |x_1| \le 2,\ |x_2| \ge 2\},\quad \mathcal{O}_C = \{x \in X \mid |x_1| < 1\},$$

$$\mathcal{O}_L = \{x \in X \mid x_1 < -2\},\quad L = \{x \in X \mid -2 \le x_1 \le -1,\ |x_2| \le 2\},$$

$$\mathcal{O}_R = \{x \in X \mid x_1 > 2\},\quad R = \{x \in X \mid 1 \le x_1 \le 2,\ |x_2| \le 2\},$$

$$a = L \cap cl(\mathcal{O}_L),\ b = L \cap cl(\mathcal{O}_C),\ c = R \cap cl(\mathcal{O}_C),\ d = R \cap cl(\mathcal{O}_R).$$

Consider a continuous mapping $\varphi : L \cup R \to X$ and suppose that

$$\varphi(a \cup d) \subset \mathcal{O}_R\,,\ \varphi(b \cup c) \subset \mathcal{O}_L \quad \textit{and} \quad \varphi(L \cup R) \subset X \setminus E \tag{3}$$

or

$$\varphi(a \cup c) \subset \mathcal{O}_R\,, \varphi(b \cup d) \subset \mathcal{O}_L \quad \textit{and} \quad \varphi(L \cup R) \subset X \setminus E. \tag{4}$$

See Fig. 1. Then condition (2) is satisfied.

Proof. The proof mimics the derivation of Miranda's Theorem (see e.g. in [Zeidler, 1986]) from the one of Brouwer's in [Piccinini et al., 1984].

We may assume that condition (3) is satisfied. (The alternative condition (4) can be handled in a similar way. With conditions (3) and (4), Theorem 3 can be interpreted as a topological perturbation result for the U–horseshoe and the G–horseshoe, respectively.)

Set–see Fig. 2–$D = \{x \in X \mid |x_2| \le \min\{4 - |x_1|,\ 2,\ 1 + |x_1|\}\}$ and consider a continuous mapping $G : X \to X$ with the properties that

$$G(x) = x \ \text{ whenever } \ x \in L \cup R, \ \ G(\mathcal{O}_L) \subset \mathcal{O}_L,\ G(\mathcal{O}_R) \subset \mathcal{O}_R,$$

$$G(X) \subset D, \ \text{ and } \ (G(x))_1 = x_1 \ \text{ whenever } x \in X \text{ with } |x_1| \le 2\,.$$

For $x \in L \cup R$, define $\delta(x) = G(\varphi(x))$. By a simple compactness argument, there exists a $\mu > 0$ such that

$$\delta(a \cup d) \subset \{x \in D \mid x_1 \ge 2 + \mu\},\ \delta(b \cup c) \subset \{x \in D \mid x_1 \le -2 - \mu\},$$

$$\delta(L \cup R) \subset \{x \in D \mid |x_2| \le 2 - \mu\}.$$

Again, by compactness and continuity, there exists a $\nu \in (0, \frac{1}{2})$ such that

$$\delta(L_{L,\nu} \cup R_{R,\nu}) \subset \{x \in D \mid x_1 \ge 2\}, \ \ \delta(L_{R,\nu} \cup R_{L,\nu}) \subset \{x \in D \mid x_1 \le -2\}$$

$$\text{where} \quad L_{L,\nu} = \{x \in L \mid x_1 \le -2 + \nu\}, \ \ R_{R,\nu} = \{x \in R \mid x_1 \ge 2 - \nu\}$$

$$\text{and} \quad L_{R,\nu} = \{x \in R \mid x_1 \ge -1 - \nu\}, \ \ R_{L,\nu} = \{x \in L \mid x_1 \ge 1 + \nu\}.$$

Let δ_i denote the coordinate functions of δ, $i = 1, 2$. Observe that $|\delta_1(x)| \le 4$ and $|\delta_2(x)| \le 2$ for each $x \in L \cup R$. With φ replaced by δ, mapping $\Delta_\alpha : Q_\alpha \to Q_\alpha$ is defined by (1).

Given a multiindex α arbitrarily, we claim that equations $q = \Phi_\alpha(q)$ and $q = \Delta_\alpha(q)$ have exactly the same solutions in Q_α. In other words, $q_k = G(\varphi(q_{k-1}))$ with $q_k \in L \cup R$, $k = 0, 1, \ldots, N$ if and only if $q_k = \varphi(q_{k-1})$ with $q_k \in L \cup R$, $k = 0, 1, \ldots, N$ (with the convention that $q_{-1} = q_N$ and $q_{N+1} = q_0$). The 'if part' follows simply by a coordinatewise composition with G. In order to prove the 'only if part', observe first that

$$\varphi(q_{k-1}) \in X \setminus E \subset (\mathcal{O}_L \cup \mathcal{O}_R \cup \mathcal{O}_C) \cup (L \cup R).$$

However, $G(\varphi(q_{k-1})) = q_k \in L \cup R$ for some $\varphi(q_{k-1}) \in \mathcal{O}_L \cup \mathcal{O}_R \cup \mathcal{O}_C$ is excluded by the properties of G. Hence $\varphi(q_{k-1}) \in L \cup R$ and $G(\varphi(q_{k-1})) = \varphi(q_{k-1})$, $k = 0, 1, \ldots, N$.

It remains to check that $q = \Delta_\alpha(q)$ for some $q \in Q_\alpha$. Set $\kappa = \frac{\nu}{6}$ and rewrite the fixed point equation $q = \Delta_\alpha(q)$ as the $2(N+1)$-dimensional system

$$q_{k,1} = q_{k,1} + \beta_k \kappa[\delta_1(q_k) - q_{k+1,1}], \ \ q_{k,2} = q_{k,2} + \kappa[\delta_2(q_{k-1}) - q_{k,2}], \qquad (5)$$

where $q_k = (q_{k,1}, q_{k,2}) \in Q_{\alpha_k}$ and $\beta_k = 1$ if $\alpha_k = 0$ and -1 if $\alpha_k = 1$, $k = 0, 1, \ldots, N$. It is somewhat lengthy but straightforward to check that

the compact convex set Q_α is mapped into itself by the operator on the right-hand side of (5), and thus the conditions of Brouwer's fixed point theorem are satisfied. In fact,

$$|q_{k,2} + \kappa[\delta_2(q_{k-1}) - q_{k,2}]| \leq (1-\kappa)|q_{k,2}| + \kappa|\delta_2(q_{k-1})| \leq (1-\kappa)2 + \kappa \cdot 2 = 2$$

whenever $q \in Q_\alpha$, $k = 0, 1, \ldots, N$. As for the first coordinate of q_k, we distinguish two cases according to $q_k \in L$ or $q_k \in R$. Case $q_k \in L$ is equivalent to $\beta_k = 1$ and consists of the three subcases $q_k \in L_{L,\nu}$, $q_k \in L_{R,\nu}$, and $q_k \in L \setminus (L_{L,\nu} \cup L_{R,\nu})$. If $q_k \in L_{L,\nu}$, then $\delta_1(q_k) - q_{k+1,1} \in [0, 6]$ and thus

$$q_{k,1} + \beta_k \kappa[\delta_1(q_k) - q_{k+1,1}] \in [-2, -2 + \nu + 6\kappa] \subset [-2, -1].$$

If $q_k \in L_{R,\nu}$, then $\delta_1(q_k) - q_{k+1,1} \in [-6, 0]$ and thus

$$q_{k,1} + \beta_k \kappa[\delta_1(q_k) - q_{k+1,1}] \in [-1 - \nu - 6\kappa, -1] \subset [-2, -1].$$

Finally, if $q_k \in L \setminus (L_{L,\nu} \cup L_{R,\nu})$, then $\delta_1(q_k) - q_{k+1,1} \in [-6, 6]$ and thus

$$q_{k,1} + \beta_k \kappa[\delta_1(q_k) - q_{k+1,1}] \in [-2 + \nu - 6\kappa, -1 - \nu + 6\kappa] = [-2, -1].$$

Case $q_k \in R$ (i.e. the remaining subcases $q_k \in R_{L,\nu}$, $q_k \in R_{R,\nu}$, and $q_k \in R \setminus (R_{L,\nu} \cup R_{R,\nu})$ can be settled similarly. □

Replacing the respective arguments in [Mischaikow & Mrozek, 1995], [Zgliczynski, 1997a], [Zgliczynski, 1997b] by the Miranda approach we used in proving Theorem 3, we see that in the by now classical computer-assisted proofs of horseshoe-type chaos in the Lorenz, Rössler, and Hénon systems, algebraic-topological techniques are not necessary. The application of Brouwer's fixed point theorem suffices. This holds true for the Sharkovski-type results on higher-dimensional small perturbations of one-dimensional mappings in [Zgliczynski, 1999] as well.

2.3 An example

Together with Theorem 1, also Theorem 3 is of entirely topological character. Let h be a self–homeomorphism of $X = \mathbf{R}^2$. Replacing $S = X, E, \mathcal{O}_C, \mathcal{O}_L, L, \mathcal{O}_R, R$, a, b, c, d resp. φ by $h(S)$ resp. $h\varphi h^{-1}$, Theorem 3 remains valid and $\varphi : L \cup R \to X$ has a horseshoe–type L–R chaos in X. It is also clear that set E in Theorem 3 can be replaced by the larger set $\{x \in X \mid |x_1| \leq 2, |x_2| \geq 2\}$.

Such a homeomorphic version of Theorem 3 was used by [Zgliczynski, 1997a] to point out that the seventh iterate of the well–known Hénon mapping $\mathcal{H} : \mathbf{R}^2 \to \mathbf{R}^2$, $(x_1, x_2) \to (1 + x_2 - Ax_1^2, Bx_1)$, with the classical parameters $A = 1.4$ and $B = 0.3$, has a horseshoe–type L–R chaos.

In what follows we describe his construction. With parameters $0 < E_{2,top} < E_{1,bottom}$ and $E_{1,left} < E_{2,right}$ specified later, set

$$E_1 = \{(x_1, x_2) \in \mathbf{R}^2 \mid x_1 \geq E_{1,left}\ ,\ x_2 \geq E_{1,bottom}\},$$

$$E_2 = \{(x_1, x_2) \in \mathbf{R}^2 \mid x_1 \leq E_{2,right}\ ,\ 0 \leq x_2 \leq E_{2,top}\}.$$

With $E_{1,left} \leq x_1^a < x_1^b < x_1^c < x_1^d \leq E_{2,right}$ and $0 < \tan\alpha$ specified later, define the straight line segments

$$\sigma = \{(x_1, x_2) \in \mathbf{R}^2 \mid E_{2,top} \leq x_2 = E_{2,top} + (x_1 - x_1^\sigma) \cdot \tan\alpha \leq E_{1,bottom}\},$$

$\sigma = a, b, c, d$. Let Q_0 and Q_1 be the parallelograms between E_1 and E_2 with parallel sides a, b and c, d, respectively. Note that α is the lower left angle of these parallelograms. Let $E = E_1 \cup E_2$. Finally, let $\mathcal{O}_L$ and $\mathcal{O}_R$ be the unbounded components of the open set $\mathbf{R}^2 \setminus (E \cup Q_1 \cup Q_2)$ containing the points $(-1 + E_{1,left}, E_{1,bottom})$ and $(1 + E_{2,right}, 0)$, respectively. See Fig. 3.

Example 1 *Taking $E_{2,top} = 0.01$, $E_{1,bottom} = 0.28$, $E_{1,left} = 0.4$, $E_{2,right} = 0.64$, $A = 1.4$, $B = 0.3$, $\tan\alpha = 2$, $x_1^a = 0.460$, $x_1^b = 0,556$, $x_1^c = 0.558$, $x_1^d = 0.620$, [Zgliczynski, 1997a] checked by interval arithmetic based rigorous computation that the subset relations*

$$\mathcal{H}^7(a \cup d) \subset \mathcal{O}_R,\ \mathcal{H}^7(b \cup c) \subset \mathcal{O}_L \quad \textit{and} \quad \mathcal{H}^7(Q_0 \cup Q_1) \subset \mathbf{R}^2 \setminus E \qquad (6)$$

are satisfied. See Fig. 4. Applying his version of Theorem 3 above, Zgliczynski arrived at the standard horseshoe dynamics embedded in the seventh iterate of mapping $\mathcal{H}$.

In our terminology, he concluded that $\mathcal{H}^7$ has a horseshoe–type L–R chaos with $L = Q_0$ and $R = Q_1$. Though the concept of L(left)–R(right) chaos refers only to encodings with doubly–infinite 0–1 sequences (and not to semiconjugacies with the shift operator on symbol spaces), we think it does express what we see on the computer screen in natural terms of the dynamics, in a vividly descriptive way.

3 Computer Procedures in Proving Chaos

In order to check subset relations of the form $\mathcal{T}(W) \subset U$ in a rigorous way, several algorithms were developped in the last decade. They form an integer part of what is called set–valued numerics and surveyed in [Dellnitz & Junge, 2002]. The key task is, however, to establish the subset relations themselves. We assume that $\mathcal{T} : \mathbf{R}^n \to \mathbf{R}^n$ is continuous, $W \subset \mathbf{R}^n$ is compact, $U \subset \mathbf{R}^n$ is open. The major assumption is that $\mathcal{T}$, W, and U depend on some vector $\lambda \in \Lambda$ of parameters where Λ is a compact subset of $\mathbf{R}^m$. The parameter vector has to be specified in such a way that the resulting subset relation $\mathcal{T}(\lambda_0)(W(\lambda_0)) \subset U(\lambda_0)$ is fulfilled. To the best of our knowledge, no general methods have been developed for this purpose in the literature so far. Successful subset relations have always been found in a trial and error interaction between computer and computer scientist.

In what follows the task of finding successful subset relations is modelled as a constrained optimization problem. The checking algorithm presented first will then be built in a framework optimization algorithm and numerical results provided.

3.1 A checking algorithm

The checking algorithm is a branch–and–bound procedure using interval arithmetic based inclusion functions [Alefeld & Mayer, 2001], [Ratschek & Rokne, 1988]. The point–to–point transformation $\mathcal{T} : \mathbf{R}^n \to \mathbf{R}^n$ is replaced by its natural interval extension $T : \mathbf{I}^n \to \mathbf{I}^n$ where $\mathbf{I}^n$ stands for the set of all closed rectangles in $\mathbf{R}^n$. Note that $\mathcal{T}(x) \in T(I)$ whenever $I \in \mathbf{I}^n$ with $x \in I$. For $I, J \in \mathbf{I}^n$, $I \subset J$ implies $T(I) \subset T(J)$. The width of the rectangle $I = \prod_{i=1}^{n} [\underline{x}_i, \overline{x}_i]$ is defined as $w(I) = \max\{|\overline{x}_i - \underline{x}_i| \;\big|\; i = 1, 2, \ldots, n\}$. For any bounded subset S in $\mathbf{R}^n$, note that $w(T(I_j)) \to 0$ holds for all interval sequences $\{I_j\}$ with $I_j \subset S$ for all $j = 1, 2, \ldots$ and $w(I_j) \to 0$. To enclose the rounding errors and to provide verified numerical results it suffices to use the so–called outward rounding that gives computer representable result intervals containing all the points of the real operations.

ALGORITHM 1 *The Checking Routine*

Inputs:
- ε: the user set limit size — threshold — of subintervals,
- W: the argument set,
- U: the aimed set for which $\mathcal{T}(W) \subset U$ is to be checked.

1. Calculate the initial interval $I \supset W$
2. Push the initial interval into the stack
3. **while** (the stack is nonempty)
4. Pop an interval I out of the stack
5. Calculate the width of I
6. Determine the widest coordinate direction
7. Calculate the transformed interval $J = T(I)$
8. **if** $I \cap W \neq \emptyset$, and the condition $J \subset U$ does not hold, **then**
9. **if** the width of interval I is less than ε **then**
10. **print** that $\mathcal{T}(W) \subset U$ is hurt by I and **stop**
11. **else** bisect I along the widest side: $I = I_1 \cup I_2$
12. push the subintervals into the stack
13. **endif**
14. **endif**
15. **end while**
16. **print** that $\mathcal{T}(W) \subset U$ is proven and **stop**

For details as well as for a formal proof of the correctness of Algorithm 1, see our parallel paper [Csendes *et al.*, 2006].

Fig. 5. belongs to the example discussed in Subsec. 2.3. The upper left quadrant portrays the parallelograms Q_0 and Q_1. The rest of Fig. 5. shows the subintervals generated by Algorithm 1 when checking that, with the parameters determined by [Zgliczynski, 1997a], the subset relations $\mathcal{T}_j(W_j) \subset U_j$ in (6), $j = 1, 2, 3$, are all satisfied. The initial interval was chosen for $[0.46, 0.755] \times [0.01, 0.28]$, the smallest interval containing $Q_0 \cup Q_1$. The threshold value was set to be $\varepsilon = 10^{-10}$. Then the three subset relations in (6) were checked one after the other. (As in [Zgliczynski, 1997a], the sets $U_1 = \mathcal{O}_R$ and $U_2 = \mathcal{O}_L$ in (6) were replaced by the smaller but more easily treatable sets $\{x_1 < E_{1,left},\ x_2 > E_{2,top}\}$ and $\{x_2 < 0\}$, respectively.) The density of the subdivision on Fig. 5. indicates subregions where the overestimation involved in the interval calculations required much refinement. For $j = 1, 2, 3$, we ended up with a covering $\{I_1^j, \ldots, I_{s_j}^j\} \subset \mathbf{I}^2$ of W_j satisfying $T_j(I_s^j) \subset U_j$ for each $s = 1, \ldots, s_j$. The CPU time was a few seconds. The depth of the stack and the number of function evaluations were (11; 273), (13; 523), and (14; 1613), respectively.

3.2 The accompanying optimization problem

Each relation $\mathcal{T}_j(W_j) \subset U_j$, $j = 1, 2, \ldots, M$ is analyzed separately. The j–th execution of Algorithm 1 may result in an interval $I_j = I_j(\lambda)$ such that

$I_j \cap W_j \neq \emptyset$ but $T_j(I_j) \subset U_j$ does not hold true. This means that the j–th execution of Algorithm 1 ends at Step 10 — let $\mathcal{J} = \mathcal{J}(\lambda) = \{j_1, \ldots, j_\ell\} \subset \{1, 2, \ldots, M\}$ denote the set of such indices. Otherwise, for $j \notin \{j_1, \ldots, j_\ell\}$, the j–th execution of Algorithm 1 ends at Step 16.

Consider the optimization problem

$$\min_{\lambda \in \Lambda} g(\lambda) \qquad \text{where} \quad g(\lambda) = p\left(\sum_{j \in \mathcal{J}(\lambda)} \max_{v \in T_j(I_j(\lambda))} \inf_{u \in U_j(\lambda)} |u - v| \right) . \quad (7)$$

Here $I_j(\lambda)$ is the interval returned by the checking routine for $j \in \mathcal{J}(\lambda)$ (and the empty set for $j \notin \mathcal{J}(\lambda)$), $\Lambda \subset \mathbf{R}^m$ is the search set (the compact set of admissible parameter values), and $p : \mathbf{R} \to \mathbf{R}$ is a penalty function. Note also that $\max_{v \in T_j(I_j(\lambda))} \inf_{u \in U_j(\lambda)} |u - v|$ is the Hausdorff distance of the transformed subinterval $T_j(I_j(\lambda))$ to the set $U_j(\lambda)$, $j \in \mathcal{J}(\lambda)$. The computation of this Hausdorff distance can be easily accomplished provided that $n = 2$ and that the boundary of each $U_j(\lambda)$ consists of a moderate number of finite or infinite straight line segments.

Motivated by earlier experiences [Csendes, 1988], [Markót & Csendes, 2005], our favorite choice for the penalty function in (7) is to take a nonnegative value proportional to how much the given condition is hurt, plus a fixed penalty term in case at least one of the constraints is not satisfied. Thus, we let $p(r) = r + 1$ if r is positive and $p(r) = 0$ otherwise. If an optimization algorithm leads to a parameter vector λ_0 with $g(\lambda_0) = 0$, then—at the same time—the built–in checking routine provides a guaranteed reliability computational proof of the respective subset relations $\mathcal{T}_j(\lambda_0)(W_j(\lambda_0)) \subset U_j(\lambda_0)$, $j = 1, 2, \ldots, M$. Unfortunately, due to the high degree of nonlinearity of the problem, it is well possible that the output of the optimization algorithm is inconclusive, even if $\min_{\lambda \in \Lambda} g(\lambda) = 0$.

For a detailed discussion of this optimization model and of the relevant techniques of global optimization, see our parallel paper [Csendes *et al.*, 2006]. For the general theory of constraint satisfaction problems, see [Neumaier, 2004].

3.3 Numerical results

We restrict ourselves to the two–dimensional case and remain in the general setting of the example discussed in Subsec. 2.3. Our aim is to find horseshoe–type L–R chaos for $k \leq 6$ iterates of the family of Hénon mappings. (Case $k \geq 8$ will be investigated in a separate paper.)

The computer–aided results were achieved both in the Linux and in the Cygwin environment, on an average personal computer. We used the C–XSC [Klatte *et al.*, 1993] programming language supporting interval arithmetic.

The successful parameter values—for $\mathcal{H}^6$, $\mathcal{H}^4$, and $\mathcal{H}^2$ with the classical parameters $A = 1.4$ and $B = 0.3$—found below are, of course, in full conformity with the inner structure of the respective Hénon mappings. The homoclinic saddle point $P = (0.63..., 0.18...) \in \mathbf{R}^2$ of $\mathcal{H}$ is always in $Q_0 \cup Q_1$. With a fairly good approximation, the unstable eigenvalue direction at P is horizontal whereas $\tan(\alpha) = 2$ is not too far from the tangent of the stable eigenvector.

3.3.1 Stability of Example 1 with respect to the parameters

Keeping Zgliczynski's sets E_1, E_2, Q_0 and Q_1 fixed, the subset relations in (6) are satisfied for parameters

$$(A, B) \in [1.377599,\ 1.401300] \times [0.277700,\ 0.310301].$$

Slightly better results are shown on Fig. 6. On the other hand, if the angle parameter is allowed to be changed (while the remaining 10 parameters are kept constant), the subset relations in (6) are satisfied for $1.964775 \leq \tan(\alpha) \leq 2.067229$.

Similarly, if only parameters x_1^a, x_1^b, x_1^c (satisfying $x_1^b < x_1^c$), and x_1^d are subject to changes, existence of horseshoe–type L–R chaos is proved for points of the four–dimensional parameter interval

$$x_1^a \in [0,455609,\ 0.516032],$$

$$x_1^b, x_1^c \in [0.544512,\ 0.590421],$$

$$x_1^d \in [0.605679,\ 0.64].$$

This latter task required 23 minutes CPU time.

The technique with which the above results were obtained is an earlier interval arithmetic procedure [Csendes *et al.*, 1995] worked out for solving tolerance optimization problems.

3.3.2 Horseshoe–type L–R chaos for $\mathcal{H}^k$, $k = 6, 4, 2$

We have applied the global optimization model introduced in Subsec. 3.2 for the next plausible case, the sixth iterate of the Hénon mapping. After some

LO	ZO	MV	FE	PE	T
12	0	1.0947353	14,019	5,149	20
12	2	0.0	11,904	2,603	12
12	0	1.0760938	14,660	5,596	21
12	0	1.0000043	13,325	4,092	15
12	0	1.0395415	13,700	5,044	24
12	0	1.0255977	13,067	3,758	15
12	0	1.0402164	13,622	4,561	23
12	2	0.0	12,721	3,532	13
12	2	0.0	12,935	3,733	16
12	1	0.0	13,920	4,639	19

Table 1: $k = 6$: Numerical results of the search runs for identifying suitable parameters. Here LO stands for number of local optima found, ZO for the number of zero optimum values, MV for the smallest local minimum value found, FE for the number of function evaluations, PE for the number of penalty function evaluations, and finally T for the CPU time used in minutes.

experimentation, the search domain for the parameters to be optimized was chosen as

$$E_{1,bottom} \in [0.1,\ 0.3], \quad \tan(\alpha) \in [0.5,\ 3.0], \quad x_1^a, x_1^b, x_1^c, x_1^d \in [0.10,\ 0.90],$$

while $E_{1,left}$ resp. $E_{2,right}$ were identified with x_1^a resp. x_1^d, and the remaining 3 parameters were the same as in Subsec. 2.3. The setting for the global optimization algorithm was the following: in each iteration round we have generated 5000 sample points with uniform distribution over the search domain, out of which the 10 best were kept for the local search phase, a version of the gradient method. The stopping criterion threshold for the local search was set to 15 digits. This iteration was repeated until no new local minimum has been found. The ε stopping criterion parameter value for the checking algorithm was set to 0.001. This relatively large value enabled the algorithm to run quicker, to use a modest amount of CPU time. Table 1 presents the numerical results of the search runs for identifying suitable parameters.

One example of the obtained optimized parameter values is

$$E_{1,bottom} = 0.2491759, \quad \tan(\alpha) = 1.9645949,$$

$$x_1^a = 0.5168849,\ x_1^b = 0.60155904,\ x_1^c = 0.62133119,\ x_1^d = 0.76488491.$$

LO	ZO	MV	FE	PE	T
4	0	1.0661465	33,742	17,396	43
1	0	1.1325119	24,730	21,820	172
1	0	1.00097	16,420	6,130	8
3	0	1.0929769	42,936	28,098	52
2	0	1.0004248	22,566	11,696	28
7	1	0.0	49,673	22,770	35
6	0	1.0006516	31,046	20,670	28
1	0	1.3397567	16,250	5,760	23
2	0	1.0003695	20,752	10,637	27
6	0	1.0007408	40,688	14,684	13

Table 2: $k = 3$: Numerical results of the search runs for identifying suitable parameters. The notation is the same as in Table 1.

See Fig. 7. Although the clustering global optimization algorithm applied intends to locate different local minima, all the found global optimum solutions were similar to the one given above. (This means that each setting with horseshoe–type L–R chaos we found for $\mathcal{H}^6$ corresponds to the same returning portion of the unstable manifold of the homoclinic saddle point P. All the obtained chaotic parallelogram configurations seem to be deformable into each other along a one–parameter path of two parallelograms with horseshoe–type L–R chaos.)

It is known [Szymczak, 1997] that both $\mathcal{H}^5$ and $\mathcal{H}^3$, equipped with the classical parameters, have exactly two fixed points. Consequently, in order to find horseshoe–type L–R chaos for them, one has to vary the (A, B)–parameters, too. As for $\mathcal{H}^3$, keeping only parameter $E_{2,top} = 0.01$ fixed, the optimization algorithm resulted in horseshoe–type L–R chaos at the parameter values

$$E_{1,bottom} = 0.18937143,\ E_{1,left} = 0.21673342,\ E_{2,right} = 0.84386042,$$

$$A = 2.5569088,\ B = 0.15963498,\quad \tan(\alpha) = 3.3579163,$$

$$x_1^a = 0.29188440,\ x_1^b = 0.53887296,\ x_1^c = 0.74663494,\ x_1^d = 0.84359572.$$

Characteristics of the numerical results are presented in Table 2.

For this run the distances for the hurt conditions in the penalty function were multiplied by 100. Case $\mathcal{H}^5$ was settled already in our parallel paper [Csendes *et al*, 2006].

Now we return to the classical parameters $A = 1.4$, $B = 0.3$ and consider the fourth iterate $\mathcal{H}^4$. We leave Zgliczynski's parallelograms completely and work with 16 parameters this time, the coordinates of the vertices of two general quadrangles $Q_0 = L$ and $Q_1 = R$. Suggested by the position of the fixed points of $\mathcal{H}^4$, the search domains for the individual vertices of L are chosen for

$$V_{ul}^L \in [0.0,\ 0.5] \times [0.20,\ 0.25],\ V_{ur}^L \in [0.2,\ 0.6] \times [0.20,\ 0.25],$$

$$V_{ll}^L \in [0.0,\ 0.4] \times [0.01,\ 0.15],\ V_{lr}^L \in [0.2,\ 0.6] \times [0.01,\ 0.15],$$

whereas the search domains for the individual vertices of R are chosen for

$$V_{ul}^R \in [0.3,\ 0.6] \times [0.20,\ 0.25],\ V_{ur}^R \in [0.6,\ 0.8] \times [0.20,\ 0.25],$$

$$V_{ll}^R \in [0.3,\ 0.6] \times [0.01,\ 0.15],\ V_{lr}^R \in [0.6,\ 0.8] \times [0.01,\ 0.15].$$

(Here, of course, indices *ul, ur, ll, lr* stand for upper left, upper right, lower left, and lower right, respectively.) These requirements do not exclude possible overlaps and self–intersections. What we actually require is a finite number of geometric conditions on the relative position of the two quadrangles and of the four components of the forbidden set E. See Fig. 8. and cf. Fig. 2.

More precisely, we require that quadrangle L be on the left of quadrangle R and that the eight half–lines determining E be parallel to each other with common tangent $\tan(\vartheta) = 0.1$; this latter value being the result of some experimentation. Also the height order of these half–lines (in each group of four belonging to the upper resp. lower vertices of the two quadrangles) is prescribed. The fulfilment of these geometric conditions is guaranteed by adding new terms to the penalty function. The optimization algorithm ended with the existence of horseshoe–type L–R chaos and resulted e.g. in

$$V_{ul}^L = (0.16411140,\ 0.25423058),\ V_{ur}^L = (0.42592396,\ 0.23215738)\ ,$$

$$V_{ll}^L = (0.10254433,\ 0.19021336),\ V_{lr}^L = (0.31142238,\ 0.04691830),$$

as for the vertices of quadrangle L, and

$$V_{ul}^R = (0.54081838,\ 0.23803993),\ V_{ur}^R = (0.69119556,\ 0.21877527)\ ,$$

$$V_{ll}^R = (0.43871354,\ 0.03378272),\ V_{lr}^R = (0.64446463,\ 0.03638828),$$

as for the vertices of quadrangle R. See Fig. 9. Note that the local search phase may lead to a global optimum outside the search domain (which refers

LO	ZO	MV	FE	PE	T
12	10	0.0	2,733	2,709	35
12	11	0.0	2,514	2,511	31
12	9	0.0	2,738	2,737	50
12	12	0.0	1,127	1,127	16
12	11	0.0	2,737	2,733	36
12	11	0.0	1,442	1,436	16
12	10	0.0	2,865	2,862	38
12	10	0.0	2,729	2,726	59
12	10	0.0	2,649	2,644	43
12	10	0.0	2,385	2,382	49

Table 3: $k = 2$: Numerical results of the search runs for identifying suitable parameters. The notation is the same as in Table 1.

only to the first, random part of the optimization algorithm). This explains why the upper left vertex V_{ul}^L of quadrangle L above does not belong to the search rectangle $[0.0,\ 0.5] \times [0.20,\ 0.25]$.

The method we used in handling $\mathcal{H}^4$ works for the second iterate as well. The optimization algorithm ended with the existence of horseshoe–type L–R chaos for $\mathcal{H}^2$ and resulted e.g. in

$$V_{ul}^L = (-0.95008818,\ 0.38966840),\ V_{ur}^L = (-0.11192965,\ 0.33756351),$$

$$V_{ll}^L = (-0.92886824,\ 0.25677498)\ ,\ V_{lr}^L = (-0.13972836,\ 0.21535493),$$

$$V_{ul}^R = (-0.01309659,\ 0.33113756),\ V_{ur}^R = (0.70239604,\ 0.18263519)\ ,$$

$$V_{ll}^R = (-0.13451910,\ 0.20890361),\ V_{lr}^R = (0.63453236,\ 0.02108996).$$

See Fig. 10. Characteristics of the numerical results are presented in Table 3. For this run the number of sample points in the global search phase of the optimization algorithm was taken for 500. The relatively small search domains (squares with sidelength of §0.1§) were chosen after some preliminary experimentation.

There is very strong numerical evidence that the classical Hénon mapping $\mathcal{H}$ itself has no horseshoe–type L–R chaos. The argument is based on the concept of the topological entropy H. By an abstract result of [Newhouse, 1988], $H(\mathcal{H}) \leq \log 2 \approx 0.69$. All numerical experiments suggest that $H(\mathcal{H}) < 0.47$. This latter inequality—if rigorously confirmed—would

imply that $\mathcal{H}$ had no horseshoe–type L–R chaos (because the topological entropy of any continuous mapping with horseshoe–type L–R chaos is at least $\log 2$). By a recent result of [Galias, 2002], $H(\mathcal{H}) > 0.43$. The existence of horseshoe–type L–R chaos for $\mathcal{H}^2$ established in the previous paragraph implies that $H(\mathcal{H}) \geq 2^{-1} \log 2 > 0.34$. This is much worse than the lower bound in [Galias, 2002] but slightly better than the one obtained by [Galias & Zgliczynski, 2001].

4 Summary

We have shown that the task of finding regions with horseshoe-type dynamical behaviour reduces to an interval arithmetic based constraint optimization problem. This methodology has led to a pair of quadrangles on which the k-th iterate of the classical Hénon mapping (for $k = 7, 6, 4, 2$, respectively) is at least as complicated as the shift operator on two symbols.

Our approach is, in principle, fully automatic. However, the more a priori information on the dynamics exploited, the smaller the starting search region, together with the computational time necessary.

We hope that optimization methods within dynamical systems theory will play an increasingly important role in locating and proving chaotic behaviour in the future, esp. for enlarging the parameter set of chaos via tolerance optimization as well as—in order to find more complex symbolic dynamics—for adding a new (topological) rectangle to an existing configuration of rectangles.

Acknowledgments

The authors are indebted to one of the referees for her/his valuable suggestions.

This work has been partially supported by the Bilateral Austrian-Hungarian project öu56011 as well as by the Hungarian National Science Foundation Grants OTKA No. T 037491, T 032118, T 034350, T 048377, and T 046822.

References

[1] Alefeld, G. & Mayer, G. [2000] "Interval analysis: Theory and applications", *J. Comput. Appl. Math.* **121**, 421–464.

[2] Csendes, T. [1988] "Nonlinear parameter estimation by global optimization — efficiency and reliability", *Acta Cybernetica* **8**, 361–370.

[3] Csendes, T., Garay, B.M. & Bánhelyi, B. [2006] "A verified optimization technique to locate chaotic regions of a Hénon system", *J. of Global Optimiz.* (accepted) Available at
`www.inf.u-szeged.hu/~csendes/henon.pdf`

[4] Csendes, T., Zabinsky, Z.B. & Kristinsdottir, B.P. [1995] "Constructing large feasible suboptimal intervals for constrained nonlinear optimization", *Annals of Operations Research* **58**, 279–293.

[5] Dellnitz, M. & Junge, O. [2002] "Set oriented numerical methods for dynamical systems", in *Handbook of Dynamical Systems* **2** ed. by Fiedler B. (North-Holland, Amsterdam) pp. 221–264.

[6] Galias, Z. [2002] "Obtaining rigorous bounds for topological entropy for discrete time dynamical systems", in *Proc. Internat. Symposium on Nonlinear Theory and its Applications,* (Xi'an, China) pp. 619–622.

[7] Galias, Z. & Zgliczynski, P. [2001] "Abundance of homoclinic and heteroclinic connections and rigorous bounds for the topological entropy of the Henon map", *Nonlinearity* **14**, 903–932.

[8] Gidea, M. & Zgliczynski, P. [2004] "Covering relations for multidimensional dynamical systems", *J. Differ. Eq.* **202**, 32–58.

[9] Klatte, R., Kulisch, U., Wiethoff, A., Lawo, C. & Rauch, M. [1993] *C–XSC — A C++ Class Library for Extended Scientific Computing* (Springer, Berlin)

[10] Markót, M.C. & Csendes, T. [2005] "A new verified optimization technique for the "Packing Circles in a Unit Square" Problems", *SIAM J. Optimization* **16**, 193–219.

[11] Mischaikow, K. & Mrozek, M. [1995] "Chaos in the Lorenz equations: a computer-assisted proof", *Bull. Amer. Math. Soc.* **32**, 66–72.

[12] Neumaier, A. [2004] "Complete Search in Continuous Global Optimization and Constraint Satisfaction", *Acta Numerica*, 271–369.

[13] Newhouse, S. [1988] "Entropy and volume", *Ergod. Theor. Dynam. Syst.* **8**, 283–299.

[14] Piccinini, L.C., Stampaccia, G. & Vidossich G. [1984] *Ordinary Differential Equations in* $\mathbf{R}^n$ (Springer, Berlin)

[15] Ratschek H. and Rokne J. [1988] *New Computer Methods for Global Optimization* (Ellis Horwood, Chichester).

[16] Robinson C. [1999] *Dynamical Systems. Stability, Symbolic Dynamics, and Chaos* (RCR Press, Boca Raton)

[17] Szymczak, A. [1997] "A combinatorial procedure for finding isolated neighbourhoods and index pairs", *Proc. R. Soc. Edinb. A* **127**, 1075–1088.

[18] Tucker, W. [1999] "The Lorenz attractor exists", *C.R. Acad. Sci. Paris Sér. Math.* **328**, 1197–1202.

[19] Wiggins, S. [2003] *Introduction to Applied Nonlinear Dynamical Systems and Chaos* (Springer, Berlin)

[20] Wójcik, K. & Zgliczynski, P. [2000] "Isolated segments, fixed point index, and symbolic dynamics", *J. Differ. Eq.* **161**, 245–288.

[21] Zeidler, E. [1986] *Nonlinear Functional Analysis and its Applications. I. Fixed-point Theorems* (Springer, Berlin)

[22] Zgliczynski, P. [1996] "Fixed point index for iterations of maps, topological horseshoe and chaos", *Topol. Methods Nonlin. Anal.* **8**, 169–177.

[23] Zgliczynski, P. [1997a] "Computer assisted proof of the horseshoe dynamics in the Hénon map", *Random Comput. Dynam.* **5**, 1–17.

[24] Zgliczynski, P. [1997b] "Computer assisted proof of chaos in the Rössler equations and in the Hénon map", *Nonlinearity* **10**, 243–252.

[25] Zgliczynski, P. [1999] "Multidimensional perturbations of one-dimensional maps and stability of Sharkovski ordering", *Int. J. Bifurcations and Chaos* **9**, 1867–1876.

List of Figures

List of Tables

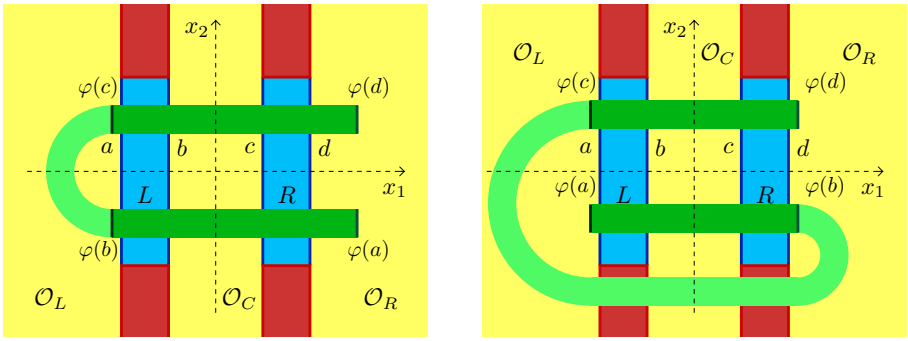

Figure 1: Two types of horseshoes. Bánhelyi et al.

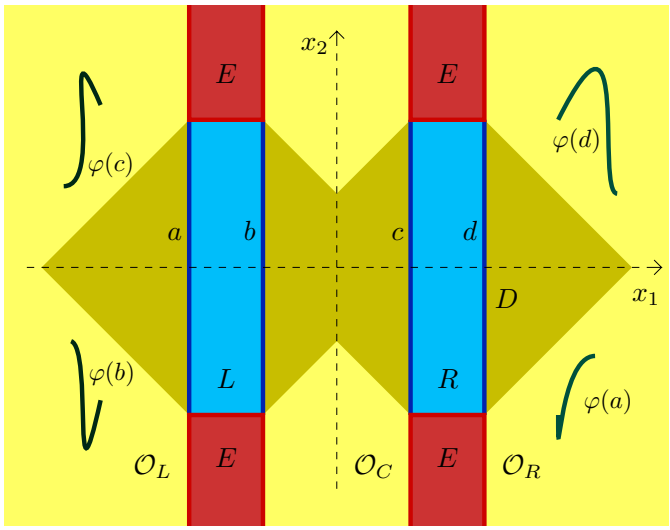

Figure 2: Illustration of the setup used in Theorem 3. Bánhelyi et al.

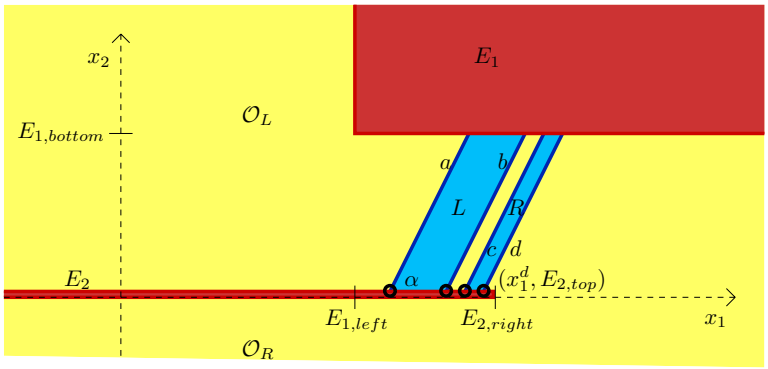

Figure 3: The notation used for the Hénon mapping investigation. Bánhelyi et al.

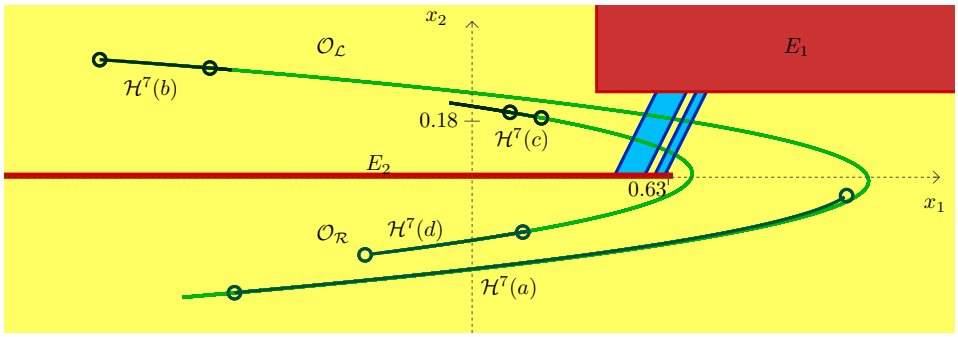

Figure 4: Illustration of the H^7 transformation with the chaotic region of two parallelograms. Bánhelyi et al.

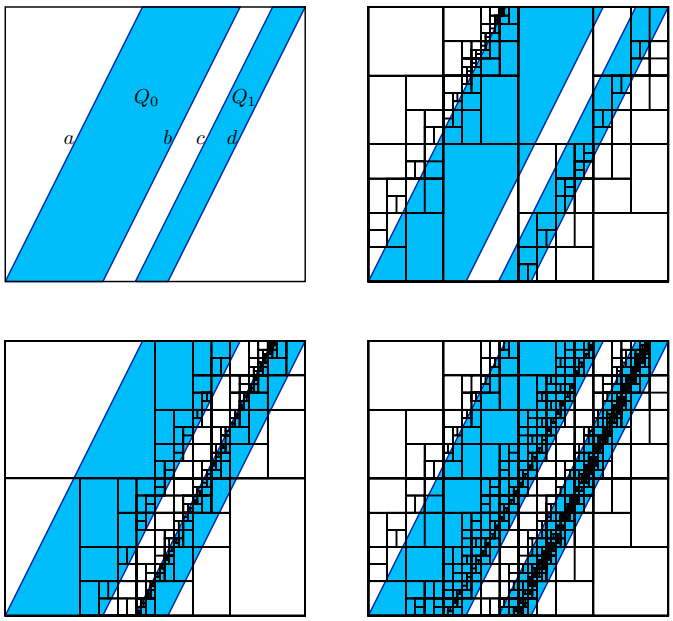

Figure 5: The parallelograms and the starting interval covered by the verified subintervals for which either the given condition holds (in the order of mentioning in Example 1.), or they do not contain a point of the argument set. See Subsec. 2.3 for the details of the problem investigated. Bánhelyi et al.

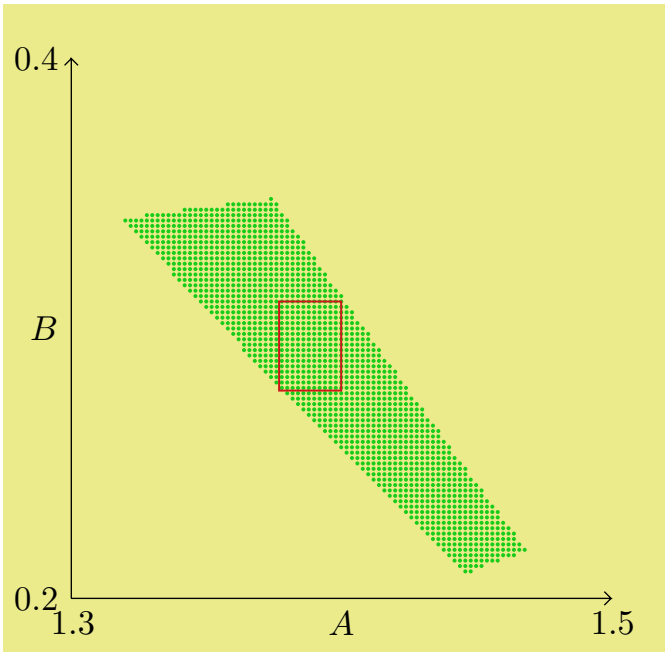

Figure 6: Illustration of the obtained interval containing only such A and B values that ensure horseshoe-type chaos in Zgliczynski's two parallelograms. Those grid points that also fulfill the conditions are denoted by small circles. Bánhelyi et al.

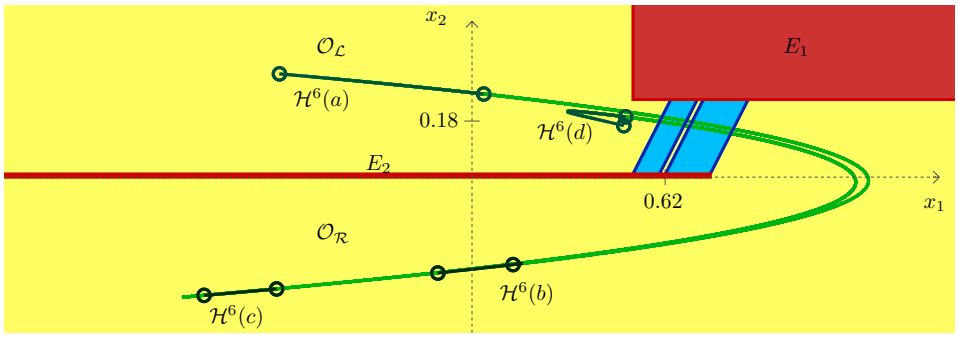

Figure 7: Illustration of the H^6 transformation with the chaotic region of two parallelograms. Bánhelyi et al.

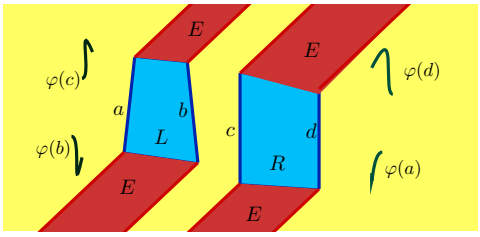

Figure 8: Illustration of the setting for the two general quadrangles. Bánhelyi et al.

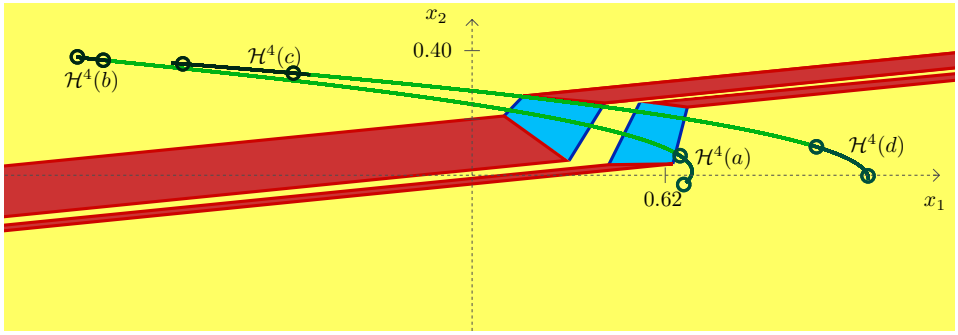

Figure 9: Illustration of the H^4 transformation with the chaotic region of two quadrangles. Bánhelyi et al.

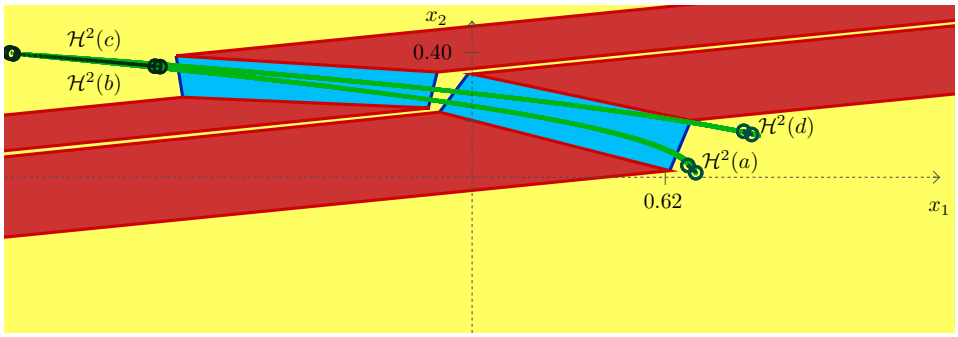

Figure 10: Illustration of the H^2 transformation with the chaotic region of two quadrangles. Bánhelyi et al.